GEOMETRIC COMPUTATION OF HUMAN GYRIFICATION INDEXES FROM MAGNETIC RESONANCE IMAGES

By

Shu Su

Tonya White

**Marcus Schmidt**

Chiu-Yen Kao

and

Guillermo Sapiro

INSTITUTE FOR MATHEMATICS AND ITS APPLICATIONS
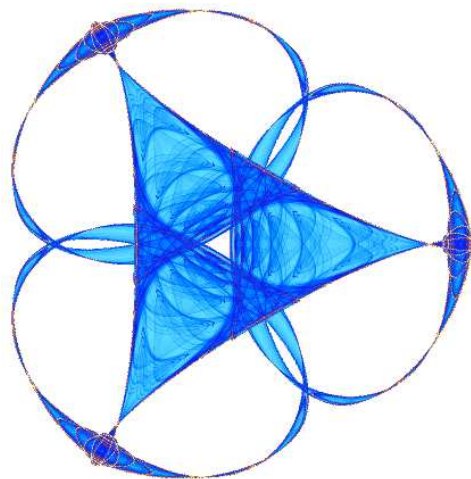
		Form Approved
Report Documentation Page		OMB No. 0704-0188

Public reporting burden for the collection of information is estimated to average 1 hour per response, including the time for reviewing instructions, searching existing data sources, gathering and maintaining the data needed, and completing and reviewing the collection of information. Send comments regarding this burden estimate or any other aspect of this collection of information, including suggestions for reducing this burden, to Washington Headquarters Services, Directorate for Information Operations and Reports, 1215 Jefferson Davis Highway, Suite 1204, Arlington VA 22202-4302. Respondents should be aware that notwithstanding any other provision of law, no person shall be subject to a penalty for failing to comply with a collection of information if it does not display a currently valid OMB control number.

1. REPORT DATE **APR 2009**	2. REPORT TYPE	3. DATES COVERED **00-00-2009 to 00-00-2009**
4. TITLE AND SUBTITLE **Geometric Computation of Human Gyrification Indexes from Magnetic Resonance Images**		5a. CONTRACT NUMBER
		5b. GRANT NUMBER
		5c. PROGRAM ELEMENT NUMBER
6. AUTHOR(S)		5d. PROJECT NUMBER
		5e. TASK NUMBER
		5f. WORK UNIT NUMBER
7. PERFORMING ORGANIZATION NAME(S) AND ADDRESS(ES) **University of Minnesota,Institute for Mathematics and Its Applications,Minneapolis,MN,55455-0436**		8. PERFORMING ORGANIZATION REPORT NUMBER
9. SPONSORING/MONITORING AGENCY NAME(S) AND ADDRESS(ES)		10. SPONSOR/MONITOR'S ACRONYM(S)
		11. SPONSOR/MONITOR'S REPORT NUMBER(S)
12. DISTRIBUTION/AVAILABILITY STATEMENT **Approved for public release; distribution unlimited**		
13. SUPPLEMENTARY NOTES		
14. ABSTRACT **see report**		
15. SUBJECT TERMS		

16. SECURITY CLASSIFICATION OF:			17. LIMITATION OF ABSTRACT **Same as Report (SAR)**	18. NUMBER OF PAGES **47**	19a. NAME OF RESPONSIBLE PERSON
a. REPORT **unclassified**	b. ABSTRACT **unclassified**	c. THIS PAGE **unclassified**			

Standard Form 298 (Rev. 8-98)
Prescribed by ANSI Std Z39-18

Geometric Computation of Human Gyrification Indexes from Magnetic Resonance Images

Shu Su[1]
Tonya White [3,4,5,6]
Marcus Schmidt [3]
Chiu-Yen Kao [1,2]
Guillermo Sapiro [7]

[1] Department of Mathematics
[2] Mathematical Biosciences Institute
The Ohio State University
[3] Division of Child and Adolescent Psychiatry
[4] Center for Neurobehavioral Development
[5] Center for Magnetic Resonance Research
University of Minnesota
[6] Department of Child and Adolescent Psychiatry,
Erasmus Medical Center, Rotterdam, Netherlands
[7] Department of Electrical and Computer Engineering,
University of Minnesota, Minneapolis, MN

Short Title:　Geometric Computation of Gyrification Indexes

<u>**Corresponding Author:**</u>
Chiu-Yen Kao
Department of Mathematics
Mathematical Biosciences Institute
The Ohio State University
231 West 18th Avenue
Columbus, OH 43210
Tel. 614.292.8609
Fax. 614.292.1479

Abstract

Human Brains are highly convoluted surfaces with multiple folds. To characterize the complexity of these folds and their relationship with neurological and psychiatric conditions, different techniques have been developed to quantify the folding patterns and gyrification of the brain. In this work, we propose a new geometric approach to measure the local gyrification of human brains from magnetic resonance images (MRI). This approach is based on intrinsic 3D measurements that relate the local brain surface area to the corresponding area of a tightly wrapped sheet. These quantities are efficiently and accurately computed solving geometric partial differential equations. The presentation of the geometric framework is complemented with experimental results for brain complexity in typically developing children and adolescents. Using this novel approach, we provide evidence for developmental alterations in brain surface complexity throughout childhood and adolescence.

1 Introduction

The cortical surface of a human brain evolves from a smooth, or lisencephalic surface, to a highly convoluted surface during the third trimester of fetal life (Welker, 1990). This process is known as gyrification, and by the time of birth the human brain, although smaller, has an appearance very much like an adult brain. Even though a cortical surface is considered to be a topological sphere, the gyri and sulci that form the fissures and folds can be complicated (Welker, 1990). It has been suggested that a higher degree of folding of the cortical surface indicates a progressive evolution of cortical complexity in humans (Zilles et al. 1988). The increased cortical folding associated with human phylogeny has produced a highly efficient mechanism to increase cortical gray matter while optimizing a smaller overall brain size. Cortical complexity, which is considered a measure of gyrification, reveals the general organization in the human cortex and the inherent structural configuration of the brain.

It is of great interest to characterize the general brain shape and provide valuable information associated with pathology through quantitative measures. The cortical complexity has been used to evaluate abnormalities of the brain's surface morphology in various neurological and psychiatric conditions and in disorders of cognition (White and Hilgetag, 2008). Estimates of cortical complexity derived from the number of voxels which occupy the boundary between the gray matter and CSF in the prefrontal cortex have shown that abnormalities, such as smaller prefrontal volume, greater sulcal width and gyral pattern abnormalities, are present in first-episode schizophrenia (Wiegand et al. 2005). Since there is a proposed connection between development and gyrification (Armstrong et al. 1995), and between gyrification and connectivity

(Van Essen, 1997), these findings may help ascertain the underlying neurobiology of schizophrenia and other psychiatric and neurological disorders.

There is growing interest in how the human brain develops gyri and sulci, how the differences in the degree of convolutions affect brain function, and how the cortical folding evolves and whether this evolution is related to human age, gender, ethnic group or health status. These mysteries of human brain development have prompted researchers to develop measurements to quantify the degree of complexity of the cortical surface. The gyrification index (GI) proposed by Zilles et al. (Zilles et al. 1988) was developed to quantify the degree of cortical folding. Their two dimensional global measurement used an estimate of the ratio between the total outline (including sulcal folds) and the superficially exposed outline using coronal sections of postmortem brains. This measure has been applied to study both the phylogeny (Zilles et al. 1988) and ontogeny (Armstrong et al. 1995) of cortical gyrification. Brains that have higher degrees of cortical folding (i.e., increased cortical complexity) yield larger values of this GI.

Anterior to posterior maps of human GI have shown greater gyrification in the frontal, temporal, and parietal lobes of the brain (Zilles et al. 1988). However, due to the oblique orientation and manual delineation (Schaer et al. 2008; Zilles et al. 1988), the intrinsic 3D nature of the brain surface is not taken into account and this gyrification index does not completely avoid a biased estimate. For example, the GI may be altered if the slice orientation is slightly different within the same subject. Since surface morphology can be considered a two-dimensional (2D) surface in three-dimensional (3D) space, it is important to consider a full 3D gyrification index to eliminate the shortcomings of the coronal 2D approach. A number of

neuroimaging software packages are currently available to generate 3D reconstructions of human brains (eg. Freesurfer (Dale et al. 1999)[1], SurfRelax (Larsson, 2001)[2], and BrainVisa (Han et al. 2004)[3]). These software packages provide the early preprocessing stages necessary to develop a 3D gyrification index, and one such 3D technique has been recently developed (Schaer et al. 2008), following in part computational techniques developed in (Kao et al., 2007).

Previous studies have proposed reliable computational algorithms to quantify gyrification using either fully automatic or semi-automatic approaches (Magnotta et al. 1999; Schaer et al. 2008; Zilles et al. 1988). The manually generated landmark studies mentioned above defined GI as the ratio of lengths in 2D coronal slices (Zilles et al. 1988) and produced a GI value for each coronal slice of each hemisphere. A curvature-based approach introduced in (Luders et al. 2006; Schaer et al. 2008) evaluates the smoothed absolute mean curvature on parameterized cortical mesh models, revealing that females have increased gyrification in frontal, parietal, temporal, and occipital cortices compared to males. This curvature based approach found differences which were not previously identified using the traditional GI approach. More recently, a localized 3D gyrification index (lGI) (Schaer et al. 2008) was developed and applied to a group of children affected by 22q11.2 Deletion Syndrome. This technique used 3D triangulated mesh reconstructions of cortical surfaces and outer hull surfaces, and measured the amount of cortical surface buried in the sulci by constructing and relating this to a non-intrinsic sphere with different radii. The authors used the approach developed by Kao et al. (Kao et al. 2007) to

---

[1] *FreeSurfer*, see http://surfer.nmr.mgh.harvard.edu/

[2] *SurfRelax*, see http://www.cns.nyu.edu/~jonas/software.html

[3] *BrainVisa*, see http://brainvisa.info/

generate the outer hull surface and the lGI for each point on the cortical surface is obtained through a depth-weighted sum of neighboring points. We will comment on this approach after we introduce our fully geometric GI measure.

In this paper, we build upon our previous work (Kao et al. 2007) and propose a 3D geometric approach for the automatic computation of global and local gyrification indices of the human brain. By finding a geometrically corresponding region on the outer hull surface for any selected region of interest on the cortical surface, we define a 3D local GI as the area ratio between the selected region and the corresponding region of a tightly wrapped sheet. Furthermore, our 3D GI can be weighted by local quantities, i.e., curvature and sulcal depth, and is fully intrinsic and different than the method proposed by Schaer et al. (Schaer et al. 2008) in that it does not depend on a chosen radius and a corresponding non intrinsic ball to determine the region used to calculate the lGI. The incorporation of the robust sulcal depth computation developed in (Kao et al. 2007) as part of the GI measurement is important to characterize different levels of convolutions in human brains.

In Section 2, we introduce the proposed novel algorithms to calculate 3D gyrification indexes. Quantitative results for our proposed gyrification indexes, and comparison with previous approaches, are presented in Section 3. For this, we present the application of our algorithm to a population of typically developing children. Finally, we conclude the paper in Section 4 briefly describing our contributions and findings and proposing further lines of study in the area of computational approaches for measuring GI.

2 Materials and Methods

A flow chart explaining the main steps of the proposed 3D geometric GI computation algorithm is shown in Figure 1. First, a T1-weighted MRI volume is segmented into different regions, e.g., white matter (WM), gray matter (GM), and cerebral-spinal fluid (CSF) regions, using for example freesurfer (Dale et al. 1999). We consider the cortical surface represented as a triangular mesh as the input to our algorithm. Second, we construct an outer hull surface covering the sulcal regions in a shrink-wrap fashion. Third, we define the geodesic depth as the shortest distance connecting each point on the cortical pial surface to a point on the outer hull surface, the connecting path staying inside the sulcal regions, and compute the depth by using an efficient fast sweeping algorithm. Fourth, a patch on the cortical surface is selected and its boundary is extracted. Fifth, the corresponding part of the selected patch on the outer hull surface is computed. Sixth and finally, we define the local 3D GI as the ratio between the area of the patch on the cortical surface and the area of the corresponding patch on the outer hull surface. This ratio can be weighted by the local sulcal depth. We now explain each one of these steps in detail.

2.1 Surface Extraction and Depth Computation

The input of our algorithm is a T1-weighted MRI human brain volume. For skull stripping, segmentation of the brain into white matter, gray matter, and cerebrospinal fluids, and

extraction of a topologically correct triangular mesh representing the pial (GM-CSF) surface of

the cerebral cortex, we use in this work the publicly available software freesurfer (Dale et al.

1999). By T_M we denote a triangle mesh with faces $T_1, ..., T_N$; we require T_M to be a closed and

orientable 2-manifold in Euclidean 3-space. Then we use a regular grid to derive an implicit

representation of the pial surface by computing the signed distance function to the surface on a

Cartesian grid (Kao et al. 2007). By using a level set technique we compute an outer hull surface

that encloses the pial surface in a shrink-wrap type fashion. The outer hull is such that one can

still distinguish the gyri, but the sulcal regions are now "filled." Then we define a depth measure

for the pial surface as the shortest distance that connects each surface point to a point on the

outer hull surface such that the connecting path remains inside the sulcal regions. The

computational realization uses an efficient fast sweeping algorithm (Kao et al. 2005; Tsai et al.

2003; Zhao, 2005).

As shown in Figure 1(a), once we have the explicit form T_M of the pial surface, we

compute the signed distance function to the surface on a Cartesian grid. In the implicit form, the

pial surface becomes the zero level set $\{\Phi = 0\}$ of the signed distance function $\Phi : R^3 \to R$

(Osher and Sethian, 1988). The details for obtaining this signed distance function can be found in

(Kao et al. 2007).

After obtaining both an explicit triangular-mesh representation and an implicit level-set

representation on a Cartesian grid, we compute the outer hull surface using a morphological

closing operation applied to the level set function Φ (Osher and Sethian, 1988). That is, we first

move the pial surface outward by a time parameter T, and then we move the surface inward by

the same amount of time. In our algorithm, we choose $T = 10$ (mm/unit time), since T needs to be large enough to fill/close the sulcal regions and also small enough to keep the overall shape of the gyri. The governing equation is

$$\begin{cases} \Phi_t + V(t) \mid \nabla \Phi \mid = 0 \\ \Phi(x, y, z, 0) = \Phi(x, y, z), \end{cases}$$

where

$$V(t) = \begin{cases} 1, & \text{for } t < T \\ -1, & \text{for } T < t < 2T. \end{cases}$$

Thus, the implicit representation of the outer hull surface is given by

$$\Psi(x) = \min\{ \Phi(x, y, z, 2T), \Phi(x, y, z, 0)\}.$$

This minimization guarantees that the outer hull surface covers, but does not penetrate the pial surface. In Figure 1(b) we show the computed outer hull surface for the given pial surface shown in Figure 1(a).

Once we generate the outer hull surface, we apply the fast sweeping method (Kao et al. 2005; Tsai et al. 2003; Zhao, 2005) to calculate the geodesic depth for points on the pial surface. The geodesic depth we define corresponds to the shortest path from the given pial surface point to the computed outer hull which do not cross the surface of the brain (Kao et al. 2007), and thus we apply our distance computation algorithm to the restricted (CSF) region between the outer hull and the pial surface $\{\Psi \le 0 \text{ and } \Phi \ge 0\}$. In Figure 1(c), we show a top view of the bottom

part of the pial surface. The color coding corresponds to the computed geodesic depth where shallow regions are colored in blue and deep regions are colored in red.

2.2 Corresponding Region on the Outer Hull Surface Computation

In this stage, we first select a region of interest (ROI) on the pial surface. The region can be chosen using several different algorithms and can involve any sulcus or gyrus of interest. Alternatively, the region can be restricted by implementing either a depth or curvature threshold. After obtaining the ROI on the pial surface, the corresponding region on the hull surface is computed in two steps.

First, the boundary of the pial surface for the selected region is extracted. Then we sample points on this boundary and find the boundary points for the corresponding region on the computed outer hull surface. This is done following the negative gradient of the previously computed sulcal depth. We extract the paths for each starting point situated on the boundary of the selected pial region by solving the following equations, and stop when we reach the outer hull surface:

$$
\begin{aligned}
\frac{dX}{dt} &= -\nabla d \\
X(0) &= B_p^s \\
X(t) &= B_h^s,
\end{aligned}
$$

where d is the geodesic depth we computed in Section 2.1, B_p^s is a point on the boundary of the

selected region on the pial surface, and B_h^s is then the corresponding boundary point on the outer

hull surface. In this way we obtain all the corresponding boundary points on the outer hull

surface, in an intrinsic and geometric fashion, and need to close the boundary. We connect the

computed outer hull boundary points by using the shortest distance along the edges of the

triangles. An alternative choice would be to use the geodesic distance on the triangular mesh T_M

(Peyre and Cohen, 2006). Since T_M is a closed and orientable 2-manifold in Euclidean 3-space,

we can march inside it and find the triangles restricted in the constructed boundary on the outer

hull surface. The region defined by these restricted triangles corresponds, on the outer hull

surface, to the selected pial region of interest. In Figure 1(d), we show a selected region in red on

the pial surface, and in Figure 1(e) we show the computed corresponding region, shown in red on

the outer hull surface. Figure 2 illustrates the axial, coronal, and sagittal slices of the original

MRI brain volume on which we overlay the intersection curve of the pial and outer hull surfaces

of one hemisphere (in blue) with the selected sulcal region on the pial surface and the computed

corresponding region on the outer hull surface (in red).

These geometric computations form the basis needed for the gyrification indexes

presented next. Before that, we should note that in contrast with (Schaer et al. 2008), where the

intersection of an extrinsic sphere of predefined radius with the outer hall is used, our

computation of the corresponding outer hull region is completely intrinsic to the geometry of the

problem.

2.3 Gyrification Indexes

The most commonly used gyrification index was proposed by Zilles et. al. in 1988 (Zilles et al. 1988), and is defined as the ratio between the lengths of the total cortical surface and the superficially exposed cortical surface on a two dimensional slice in the coronal section,

$$\mathrm{GI}^{\,i} := \frac{L_T^i}{L_S^i},$$

where L_T^i is the length of the total cortical surface on a slice i, and L_S^i is the length of the superficially exposed cortical surface on the slice i. The mean GI of each hemisphere is then defined as

$$\overline{\mathrm{GI}} = \frac{\sum_i L_T^i}{\sum_i L_S^i},$$

where the sum runs over all the slices i. This measurement does not allow for the assessment of localized properties, including development, of the gyrification. Different theories have postulated that active, localized growth of the cortical convolutions may lead to different brain structures, e.g., regions which are developing into gyri grow at a faster rate than areas destined to be become sulci. Furthermore, recent research demonstrates that the development of different regions of the brain may result in remarkably different brain functioning, e.g., the temporal lobe is more vulnerable to insults from preterm births, with a resulting increased temporal lobe GI

(Kesler et al. 2006). Thus, reliable and accurate *localized* gyrification indexes are of great interest in the understanding of the complexity of brain folding.

A. Area-Based Gyrification Measurement

We now present the first proposed local gyrification index measurement, GI^1_{local}. Using freesurfer (Dale et al. 1999), each hemisphere is classified into 35 different sulcal and gyral regions, and a complete labeling of these 35 regions can be obtained by the automated parcellation system. We group these ROIs into six regions (see Table 1) of the human cortex: frontal lobe, parietal lobe, temporal lobe, medial temporal lobe, occipital lobe, and the cingulate gyrus.

Figure 3 shows the classification of the 6 regions on the left pial surface. We can successfully identify the corresponding 6 regions on the hull surface. For comparison, we also show the inflated left pial surface, which we obtain directly from freesurfer (Dale et al. 1999).

Our local gyrification index GI^1_{local} at each lobe is then defined as the ratio between the area of the lobe on the pial surface and the area of the corresponding region on the outer hull surface,

$$\mathrm{GI}^1_{local} := \frac{A^s_p}{A^s_h},$$

where A_p^s is the area of any selected lobe on the pial surface and A_h^s is the corresponding area on

the hull surface, computed as detailed in the previous section.

This local gyrification index GI_{local}^1 has several key features:

1. The corresponding outer hull area is naturally computed from the ROI on the pial surface,

    leading to a parameter free intrinsic GI. If we select the whole pial surface, the

    corresponding region is then the whole outer hull surface, and the gyrification index

    measurement becomes

$$\mathrm{GI}_{global}^1 = \frac{A_p}{A_h},$$

where A_p is the area of the whole pial surface, and A_h is the area of the whole outer hull

surface. If we only consider a slice of the pial surface, the surface area in 3D becomes the

slice perimeter in 2D. However, this reduction may still be different from the exact

definition of Zilles (Zilles et al. 1988), since the corresponding point on the outer hull

surface may not be on the same plane any longer. From this point of view, powerful 3D

gyrification index computation is of great importance.

2. Since all the triangles in the selected region on the pial surface are collected, all the sulcal

    information restricted to the selected area is considered.

3. The selection of the region on the pial surface can be further parceled to determine GI for

    different subregions. For instance, having calculated the depth information for each point

on the pial surface, we can define a threshold d_0 and choose a region of interest as all the points with depth $d \geq d_0$.

B. Depth-Based Gyrification Measurement

Before we extend the gyrification index GI^1_{local} to a weighted gyrification index by adding the depth information of the pial surface, we introduce a normalization of the computed depth value.

Since the absolute depth significantly depends on brain size, it is reasonable to consider the relative depth. In this way, two brains with a similar morphology, but different volumes, would have comparable gyrification index. We implement this by using d_N instead of the absolute value d,

$$d_N := \frac{d}{3V \, / \, A},$$

where the denominator $3V \, / \, A$ on the right hand side is a normalization factor based on volume V and area A (Rodriguez-Carranza et al. 2008). We can examine this normalization considering a sphere of radius R, then the normalized value for a certain depth d of folding becomes

$$d_N = \frac{d}{3\,\frac{4}{3}\,\pi R^3 \, / (4\,\pi R^2)} = \frac{d}{R},$$

and if the radius is $2R$ and the depth is $2d$, the normalized depth becomes

$$d_N = \frac{2d}{3\dfrac{4}{3}\pi(2R)^3/(4\pi(2R)^2)} = \frac{d}{R}.$$

While these two spheres have similar folding but different depths, the normalized depths are the same.

We now define the depth-based gyrification index. For any region R_p selected on the pial surface, the corresponding region on the outer hull surface is denoted by R_h. A gyrification index that considers the normalized depth information d_N can be defined as

$$\mathrm{GI}^2_{local} := \frac{\displaystyle\sum_{i=1}^{N_p} d_N^i \cdot A_p^i}{\displaystyle\sum_{j=1}^{M_h} A_h^j},$$

where N_p and M_h are the total number of triangular vertices inside the regions R_p and R_h, respectively, d_N^i is the normalized depth of the vertex i (depth to the outer hull surface as detailed before (Kao et al. 2007), A_p^i is the area of the vertex i in R_p, and A_h^j is the area of the vertex j in R_h. Our definition of the area at a vertex i (see Figure 4, cyan colored vertex) is defined in the following way. For each neighboring triangle of vertex i, we find the centroid (see Figure 4, black colored) and for each neighboring ring of vertex i, find the middle point (see Figure 4, yellow colored). Then the area at vertex i is the area sum of all such triangles formed by the vertex i, the centroid of the neighboring triangle and the middle point of the neighboring ring in the same triangle. Figure 4 illustrates this.

By adding weights to the depth of the pial surface on the numerator of GI_{local}^{2}, we are approximating the volume of the restricted part between the selected region on the pial surface and the corresponding region on the outer hull surface. Thus, the 3D local gyrification index GI_{local}^{2} is in fact a measurement of the average geodesic depth in the selected region of interest. Similar to the previously defined gyrification index, the global counterpart of GI_{local}^{2} becomes

$$\mathrm{GI}_{global}^{2} = \frac{\sum\limits_{i \in \mathrm{pia}\,l} d_{N}^{i} \cdot A_{p}^{i}}{\sum\limits_{j \in \mathrm{outer\ hull}} A_{h}^{j}}.$$

This is an approximation of the average geodesic depth of the restricted (CSF) region between the outer hull and the pial surface $\{\Psi \leq 0 \text{ and } \Phi \geq 0\}$.

C. Pointwise Gyrification Measurement

Based on the geodesic depth, Section 2.1, we now present a point-wise GI. That is, for any vertex i on the pial surface, with its corresponding normalized geodesic depth d_{N}^{i}, we define

$$\mathrm{GI}_{local}^{3}(i) := d_{N}^{i}.$$

There is a connection between this definition and GI^2_{local} , let us see this connection now.

Let us assume that the selected region of interest on the pial surface has total area A^s_p , and the

corresponding region on the outer hull surface has total area A^s_h . Then,

$$\text{GI}^2_{local} = \frac{\sum\limits_{i=1}^{N_p} d^i_N \cdot A^i_p}{\sum\limits_{j=1}^{M_h} A^j_h} = \frac{(\sum\limits_{i=1}^{N_p} d^i_N \cdot A^i_p)\sum\limits_{i=1}^{N_p} A^i_p}{\sum\limits_{j=1}^{M_h} A^j_h \sum\limits_{i=1}^{N_p} A^i_p}$$

$$= \frac{(\sum\limits_{i=1}^{N_p} d^i_N \cdot A^i_p)A^s_p}{\sum\limits_{i=1}^{N_p} A^i_p \cdot A^s_h} = \frac{\sum\limits_{i=1}^{N_p} d^i_N \cdot A^i_p}{\sum\limits_{i=1}^{N_p} A^i_p} \frac{A^s_p}{A^s_h}$$

$$= \bar{d}_N \frac{A^s_p}{A^s_h},$$

where $\bar{d}_N$ is the average geodesic depth in the selected region on the pial surface. As the selected

region gets smaller and smaller, and finally converges to the vertex i , it becomes natural to

define the local gyrification index at the vertex using its own normalized geodesic depth,

obtaining GI^3_{local} . (Note that we dropped the ratio between A^s_p and A^s_h for simplicity.)

2.4 Comparison with previous work

In comparison with (Schaer et al. 2008), our proposed GI computation method is parameter free and defines the local 3D gyrification index directly on the pial surface. In (Schaer et al. 2008), they redistribute the local gyrification index to any vertex point v_i on the pial surface by first defining the local gyrification index on the outer hull surface, and the weighting during redistributing is related to the distance between v_i and the involved vertex points $\{v_j\}$ on the outer hull surface. There are several possible disadvantages of this method: first of all, the outer hull surface is a surface generated from the pial surface, and strictly speaking, there is no gyrification index on the outer hull surface. Secondly, the extrinsic distance they use in the weighting is along the normal axis of the vertex to the outer hull surface, while our intrinsic distance is the computed geodesic depth, which is a more natural technique in defining the gyrification index (Kao et al. 2007). In addition, after Schaer et al. (Schaer et al. 2008) extract the perimeter on the region of interest on the outer hull surface, they project this perimeter to the pial surface by taking the nearest point on the pial surface, whereas our correspondence relies once again on the natural geodesic depth direction. Finally, the results from a spherical mask will depend on the radius used. Smaller spheres will have greater variability secondary to anatomical differences, whereas larger spheres will not provide a localized enough measure of gyrification and will cross boundaries into alternate regions. Nevertheless, the approach by Schaer et al. (2008) is a significant improvement over the previous 2-D GI.

2.5 Subjects

To study the development of gyrification, we implement our method on a sample of 26 typically developing children and adolescents. Subjects were stratified into three age groups, which included children (8 to 12 years old), young adolescents (13 to 15 years old), and older adolescents (16 to 19 years of age). The demographic information for the children is provided in Table 2. Socioeconomic status was determined using the Four Factor Index of Social Status (Hollingshead, 1975).

2.6 Statistical Analyses:

Evaluation of the differences in demographics was assessed using either one-way ANOVA or t-tests for continuous data and chi-square tests for categorical data. Paired t-tests were used to assess lateralization of gyrification and cortical depth measures. Measures which did not demonstrate lateralizing effects were pooled. An ANCOVA of the total sample (14 males and 12 females), with age and ICV as a covariate, was used to evaluate sex effects of sulcal depth. Measures of gyrification were evaluated between the three age groups using a one-way ANOVA.

3 Experimental Results

3.1 Demographics

There were no differences between the sex, socioeconomic status, or handedness between any of the three age groups (Table 2). In addition, when stratified into two groups by sex, there were no differences in the demographic data. An ANCOVA with age as a covariate demonstrated sex differences in the total intracranial volume ($F_{1,23} = 4.8$, $p = 0.04$), however, there were no differences in ICV between the three age groups.

3.2 Data Analysis on the Pial Surface

Before analyzing the data in detail, we present an overview of the area ratio and average normalized depth for each lobe on the pial surface. The six regions are shown in Figure 3, marked with different colors. For simplicity, in the following tables, we denote the frontal lobe by `F', the parietal lobe by `P', the temporal lobe by `T', the medial temporal lobe by `MT', the occipital lobe by `O', and the cingulate cortex by `C'.

Figure 5(a) plots the area ratio $\dfrac{A_p^s}{A_p}$ and Figure 5(b) plots the normalized average depth

$\dfrac{\sum_{i=1}^{N_p} d_N^i A_p^i}{A_p}$ for each lobe in both hemispheres for subjects in the control group. Here, the notations

are the same as we mentioned in Section 2 and the labeling names and the grouping of the sulci

for each lobe are listed in Table 1. Tables 3 and 4 list the mean value of the area ratio and the

normalized average depth for the control group. They both show no significant intrinsic

differences in the left and right hemispheres.

3.3 Data Analysis of the Outer Hull Surface

The area ratio $\dfrac{A_h^s}{A_h}$ for the corresponding region of each lobe on the outer hull surface are

shown in Figure 6 and Table 5. As expected, there are no significant differences between the

hemispheres and the corresponding ordering is as for the pial surface. This supports the

technique we designed to find correspondences between the pial surface and the outer hull.

3.4 Lateralization of Sulcal Depth and Gyrification Measures

A paired t-test found that there was significant laterality for the maximum depth for many of the major sulci. These laterality differences are shown in Table 6. As expected, the regions which demonstrate lateralizing effects are related to language regions in the temporal lobes, as well as sulci within the frontal and parietal lobes. Sulci that do not show lateralizing effects include areas related to sensory and motor functions (central sulcus and calcarine fissure). Due to these differences, lateralized measures were not pooled to assess for developmental differences in sulcal depth.

Paired t-tests found no differences in either GI^1_{local} or GI^2_{local} between the left and right frontal and temporal lobes. However, there were significant laterality effects of both GI^1_{local} and GI^2_{local} in the parietal lobe (GI^1_{local}: t = 4.8, df = 28, p < 0.0001; GI^2_{local}: t = 2.9, df = 28, p = 0.007), occipital lobe (GI^1_{local}: t = 4.6, df = 28, p < 0.0001; GI^2_{local}: t = 4.6, df = 28, p = 0.01), and the cingulate cortex (GI^1_{local}: t = 3.3, df = 28, p = 0.004; GI^2_{local}: t = 2.2, df = 28, p = 0.03). The parietal lobe had greater cortical complexity on the right, whereas the occipital lobe and cingulate cortex had greater cortical complexity on the left. In addition, laterality effects were found in the medial temporal lobes for GI^2_{local} (t = -2.4, df = 28, p = 0.02), with the left lobe having greater gyrification than the right. Due to these differences, gyrification measures were not pooled for the right and left hemispheres.

3.5 Developmental Differences in Sulcal Depth

There were relatively few differences in sulcal depth between the different age groups for the 15 major sulci that were evaluated. There were age-related differences in the maximum depth of the right middle temporal sulcus ($F_{2,21} = 4.1$, $p = 0.03$), right lateral sulcus ($F_{2,21} = 3.5$, $p = 0.05$), and a trend for the right central sulcus ($F_{2,21} = 3.2$, $p = 0.06$).

3.6 Developmental Differences in Gyrification

There were no differences in the measures of GI^1_{local} or GI^2_{local} between males and females in any of the regions of interest, thus these measures were pooled for the analyses. Age-related differences in gyrification for GI^1_{local} in the left and right hemispheres can be seen in Figure 7(a) and Figure 7(b), respectively. The GI^1_{local} decreases with age in the left ($F_{2,24} = 4.6$, $p = 0.02$) and right ($F_{2,24} = 4.9$, $p = 0.02$) frontal lobe; left ($F_{2,24} = 4.2$, $p = 0.03$) and right ($F_{2,24} = 6.8$, $p = 0.004$) medial temporal lobe. In addition, there are trend decreases in the GI^1_{local} by age in the left ($F_{2,24} = 2.6$, $p = 0.09$) and right parietal ($F_{2,24} = 2.6$, $p = 0.09$).

Fewer age-related differences were found using the gyrification measure which accounts for regional differences in sulcal depth (GI^2_{local}). Age-related differences were found in the left ($F_{2,24} = 4.1$, $p = 0.03$) and right ($F_{2,24} = 6.5$, $p = 0.006$) medial temporal lobe. In addition, trend differences were found in the left ($F_{2,24} = 3.1$, $p = 0.07$) and right ($F_{2,24} = 2.8$, $p = 0.08$) cingulate,

left parietal lobe ($F_{2,24} = 2.7$, $p = 0.09$); and the left ($F_{2,24} = 2.5$, $p = 0.10$) and right ($F_{2,24} = 3.3$, $p = 0.06$) frontal lobes.

3.7 Comparison with Existing Techniques

To compare our technique with the local gyrification index (lGI) proposed by Schaer et al. (Schaer et al. 2008), we calculated lGI results at different radii and averaged these results into the six defined brain regions. It turns out that lGI is quite sensitive to the selection of the radius of the sphere. (Radius of 20, 25, 30, and 35mm as proposed are tested.) With radii of less than 20mm, not all data could be processed using Freesurfer (Dale et al. 1999) with a resultant loss in the degrees of freedom. Table 7 lists the one-way ANOVA results for radius of 20, 25, 30, and 35mm respectively.

To illustrate this strong radii dependency, we ran a one-way ANOVA test (Table 8) to show the sensitivity. From Table 8, we can observe significant differences between radii in the frontal, parietal, and temporal lobes in both hemispheres for the three age groups. More variability appears if we do analyses using gender as a covariate while the measures GI_{local}^{1} and GI_{local}^{2} we proposed behave more stable. To have a more complete idea of the effects of lGI, we did a four-radius by three-age-group by two-region ANOVA test, which showed that there were significant effects in radius ($F_{3,1271} = 44.61$, $p < 0.0001$), age group ($F_{2,1271} = 19.03$, $p < 0.0001$) and no significance in the region side ($F_{1,1271} = 1.11$, $p = 0.29$).

3.8 Discussion

We utilized a novel gyrification index computational technique to demonstrate developmental differences in gyrification in a cohort of typically developing children and adolescents. The proposed computational method employed intrinsic 3D measurement to find gyrification indexes for a region of interest or a single point on the pial surface. It is thus able to identify local alternations in brain surface complexity.

Our results support continued molding of the surface morphology of the brain through childhood and adolescence. This same time period has been shown to be associated with a decrease in surface GM and an associated increase in the surface cerebral spinal fluid (Giedd et al. 1999; Sowell et al. 2004). It is not surprising that decreases in the underlying volume of GM, would result in an associated decrease in cortical complexity, as has been demonstrated in typically developing adults (Magnotta et al. 1999). The developmental differences in GI are localized to the later maturing structures, including the frontal and medial temporal lobes (Huttenlocher, 1982, 1990). Regions that develop earlier, such as the occipital, parietal, and lateral temporal lobes, do not demonstrate the same level of developmental differences as the frontal and medial temporal regions (Huttenlocher and Courten, 1987).

The brain has reached its peak volume by eight years of age and thus it is not surprising that there are not striking developmental differences in the depths of the major sulci. Indeed, the primary sulci are the first to develop and are associated with a greater heritability (Lohmann et al. 1999). The secondary and tertiary sulci develop later, and are more linked to environmental

factors. However, most of the primary and secondary sulci form during the third trimester of fetal life (Welker, 1990) and it is likely that restructuring and depth of the major sulci, including laterality differences, are fairly stable by eight years of age. Future studies mapping the development of the sulci, gyri and GI between birth and eight years of age will be beneficial to assess alterations of these measures as language and other cognitive processes mature.

There are limitations to the current study. We had a relatively small sample size to evaluate for developmental differences. However, the fact that significant findings were present and were consistent across measures may reflect a relatively robust measure to assess developmental differences.

4 Concluding Remarks and Discussion

Our 3D geometric approach for defining the global and local gyrification indexes naturally extends the standard way of defining the coronal 2D GI and fully utilizes the intrinsic 3D nature of human cortical surface. Classifying the cortical surface into 6 different regions and defining a simple local gyrification index on each region as the area ratio of corresponding surfaces, helps us to more carefully characterize the cortical complexity in each region and therefore provides a better way to understand the effect of each region in brain functioning. Furthermore, applying our method in a clinical study, the proposed measurement of depth-weighted local gyrification turns out to be more robust in finding the developmental differences

in children and adolescents, e.g., we observe significantly increased gyrification in the right

parietal lobe and right cingulate cortex, as well as age-rated differences in the left frontal, right

parietal and the right cingulate cortex. These findings provide some references for future study

of the relationship between gyrification and neurological and psychiatric conditions, in addition

to the development of other more advanced techniques to quantify the gyrification of the human

brain.

Since there is not one universally accepted definition for computational GI, and this is a

relatively new and ongoing research area, we conclude this discussion with some possible

alternatives that deserve further study.

From a statistical point of view, the 3D local gyrification index GI_{local}^{2} is essentially an

estimation of the first moment of the area. This motivates us to consider higher order moments.

For instance, a second central moment estimator

$$\mathrm{GI}_{local}^{4} := \frac{\sum_{i=1}^{N_p} (d_N^i - d_0) \cdot A_p^i}{\sum_{j=1}^{M_h} A_h^j},$$

where

$$d_0 = \frac{\sum_{i=1}^{N_p} d_N^i \cdot A_p^i}{\sum_{i=1}^{N_p} A_p^i},$$

is the average depth in the selected region and, evaluates the variance of the area distribution and

the third central moment estimator will then help in evaluating the skewness of the area

distribution.

The gyrification index measurement does not necessarily need to be scalar valued, we can

also consider a vectorized gyrification index measurement. For any selected region R_p on the

pial surface and the corresponding region R_h on the outer hull surface, we define (for example)

$$\mathrm{GI}\,^5_{local} = \overrightarrow{\mathrm{GI}}_{local} \quad := \quad [\,\mathrm{GI}\,^1_{local}\,, \mathrm{GI}\,^2_{local}\,]$$

$$= \quad [\frac{A_p}{A_h}, \frac{\displaystyle\sum_{i=1}^{N_p} d^i_N \cdot A^i_p}{\displaystyle\sum_{j=1}^{M_h} A^j_h}].$$

With this expression, we can evaluate the local sulci information considering both the area ratio

and the average depth of the selected region, narrowing the similarity between different regions

and providing more information for analyzing the brain complexity.

These alternatives for GI computations will be tested and reported elsewhere.

Acknowledgments

References

1. E. Armstrong, A. Schleicher, H. Omran, M. Curtis, and K. Zilles (1995): The ontogeny of human gyrification, Cerebral Cortex, vol. 5, pp. 56-63.

2. A. Dale, B. Fischl, and M. Sereno (1999): Cortical surface-based analysis I. Segmentation and surface reconstruction, NeuroImage, vol. 9, pp. 179–194.

3. D. C. van Essen (1997): A tension-based theory of morphogenesis and compact wiring in the central nervous system, Nature, vol. 385, pp. 313-318.

4. J. N. Giedd, N. O. Jeffries, J. Blumenthal et al (1999): Childhood-onset schizophrenia: progressive brain changes during adolescence, Biological Psychiatry, vol. 46, pp. 892-898.

5. X. Han, D. Pham, D. Tosun, M. Rettmann, C. Xu, and J. Prince (2004): CRUISE: Cortical reconstruction using implicit surface evolution, NeuroImage, vol. 23, pp. 997–1012.

6. A. B. Hollingshead (1975): Four factor index of social status, Unpublished manuscript, Department of Sociology, Yale University, New Haven, CT.

7. P. R. Huttenlocher, C. De Courten, L. J. Garey, H. van der Loos (1982): Synaptic development in human cerebral cortex, International Journal of Neurology, vol. 17, pp. 144-154.

8. P. R. Huttenlocher, C. De Courten (1987): The development of synapses in striate cortex of man, Human Neurobiology, vol. 6, pp.1-9.

9. P. R. Huttenlocher (1990): Morphometric study of human cerebral cortex development, Neuropsychologia, vol. 28, pp. 517-527.

10. C.-Y. Kao, S. Osher, and Y.-H. Tsai (2005): Fast sweeping methods for static Hamilton-Jacobi equations, SIAM Journal on Numerical Analysis, vol. 42, pp. 2612-2632.

11. C.-Y. Kao, M. Hofer, G. Sapiro, J. Stern, K. Rehm, and D. Rottenberg (2007): A geometric method for automatic extraction of sulcal fundi, IEEE Transactions on Medical Imaging, vol. 26, pp. 530–540.

12. S. R. Kesler, B. Vohr, K. C. Schneider, K. H. Katz, R. W. Makuch, A. L. Reiss, and L. R. Ment (2006): Increased temporal lobe gyrification in preterm children, Neuropsychologia, vol. 44, Issue 3, pp. 445-453.

13. J. Larsson (2001): Imaging vision: Functional mapping of intermediate visual processes in man, Ph.D. thesis, Karolinska Institute, Stockholm, Sweden, ISBN: 91-7349-090-3.

14. G. Lohmann, D. Y. von Cramon, H. Steinmetz (1999): Sulcal variability of twins, Cerebral Cortex, vol. 9, pp. 754-763.

15. E. Luders, P. M. Thompson, K. L. Narr, A.W. Toga, L. Jancke, and C. Gaser (2006): A curvature-based approach to estimate local gyrification on the cortical surface, NeuroImage, vol. 29, pp. 1224–1230.

16. V. A. Magnotta, N. C. ANdreasen, S. K. Schultz, G. Harris, T. Cizadlo, D. Heckel, et al (1999): Quantitative in vivo measurement of gyrification in the human brain: Changes associated with aging, Cerebral Cortex, vol. 9, pp. 151-160.

17. S. Osher and J. A. Sethian (1988): Fronts propagating with curvature dependent speed: Algorithms based on Hamilton-Jacobi formulations, Journal of Computational Physics, vol. 79, pp. 12-49.

18. G. Peyre and L. D. Cohen (2006): Geodesic remeshing using front propagation, International Journal of Computer Vision, vol. 69, Issue 1, pp. 145-156.

19. C. E. Rodriguez-Carranza, P. Mukherjee, D. Vigneron, J. Barkovich, and C. Studholme (2008): A framework for in vivo quantification of regional brain folding in premature neonates, NeuroImage, vol. 41, Issue 2, pp. 462-478.

20. M. Schaer, M. Cuadra, L. Tamarit, F. Lazeyras, S. Eliez, and J.-P. Thiran (2008): A surface-based approach to quantify local cortical gyrification, IEEE Transactions on Medical Imaging, vol. 27, no. 2.

21. E. R. Sowell, P. M. Thompson, C. M. Leonard, S. E. Welcome, E. Kan, A. W. Toga (2004): Longitudinal mapping of cortical thickness and brain growth in normal children, Journal of Neuroscience, vol. 24, pp. 8223-8231.

22. Y.-H. R. Tsai, L.-T. Cheng, S. Osher, and H.-K. Zhao (2003): Fast sweeping algorithms for a class of Hamilton-Jacobi equations, SIAM Journal on Numerical Analysis, vol. 41, no.2, pp. 659-672.

23. W. Welker (1990): Why does cerebral cortex fissure and fold? In Jones EG, Peters A (eds), Cerebral Cortex, vol. 8B. New York: Plenum Press, pp. 3-136.

24. T. White T and C. C. Hilgetag (2008): Gyrification of the human brain, In Nelson CA, Luciana M (eds), Developmental Cognitive Neuroscience. Cambridge, MA: MIT Press, pp. 35-50.

25. L. Wiegand, S. Warfield, J. Levitt, Y. Hirayasu, D. Salisbury, S. Heckers, S. Bouix, D. Schwartz, M. Spencer, C. Dickey, R. Kikinis, F. Jolesz, R. McCarley, and M. Shenton (2005): An in vivo MRI study of prefrontal cortical complexity in first-episode psychosis, American Journal of Psychiatry, vol. 162, pp. 65-70.

26. H. Zhao (2005): Fast sweeping method for eikonal equations, Mathematics of Computation, vol. 74, pp. 603-627.

27. K. Zilles, E. Armstrong, A. Schleicher, and H.-J. Kretschmann (1988): The human pattern of gyrification in the cerebral cortex, Anatomy and Embryology, vol. 179, pp. 173–179.

Table 1: Parcellation of the 35 regions into 6 regions.

lobe name	region names
Frontal	caudalmiddlefrontal, lateralorbitofrontal, medialorbitofrontal, paracentral, parsopercularis, parsorbitalis, parstriangularis, precentral, rostralmiddlefrontal, superiorfrontal, frontalpole
Parietal	inferiorparietal, postcentral, precuneus, superiorparietal, supramarginal
Temporal	bankssts, inferiortemporal, middletemporal, superiortemporal, temporalpole, transversetemporal
Medial Temporal	entorhinal, fusiform, parahippocampal
Occipital	cuneus, lateraloccipital, lingual, pericalcarine
Cingulate	caudalanteriorcingulate, isthmuscingulate, posteriorcingulate, rostralanteriorcingulate

Table 2: Demographic Information for the 26 Typically Developing Children between the ages of 8 and 19 Years of Age.

	8 to 12 Year Olds	13 to 15 Year Olds	16 to 19 Year Olds	p
Age	10.5 (1.6)	14.0 (0.87)	16.9 (1.2)	
Sex (Male / Female)	4 / 2	6 / 3	4 / 7	n.s.
Socioeconomic Status	50.7 (9.7)	49.7 (15.5)	51.1 (9.7)	n.s.

Table 3: Average area ratio of each region for subjects in the control group. 'lh' stands for the left hemisphere and 'rh' stands for the right hemisphere.

Region	F	P	T	MT	O	C
lh	0.3509	0.2265	0.1540	0.0484	0.1125	0.0364
rh	0.3533	0.2302	0.1482	0.0441	0.1164	0.0380

Table 4: Mean value of the normalized average depth of each region for subjects in the control group. `lh' stands for the left hemisphere and `rh' stands for the right hemisphere.

Region	F	P	T	MT	O	C
lh	0.1241	0.1613	0.1501	0.0800	0.1001	0.0637
rh	0.1230	0.1625	0.1507	0.0757	0.0986	0.0649

Table 5: Average area ratio of each corresponding region of each hemisphere for subjects in the control group. `lh' stands for the left hemisphere and `rh' stands for the right hemisphere.

Region	F	P	T	MT	O	C
lh	0.3750	0.1937	0.1527	0.0634	0.1180	0.0509
rh	0.3777	0.1909	0.1489	0.0598	0.1261	0.0507

Table 6: Maximum depth (in mm) for the major sulci by hemisphere and paired t-test showing lateralization.

Sulci	Maximum Depth (left)	Maximum Depth (right)	t / p
Central Sulcus	29.8 (2.4)	30.1 (2.4)	n.s.
Lateral Sulcus	34.1 (2.1)	33.5 (1.9)	2.5 / 0.02
Superior Frontal	20.1 (1.6)	19.2 (2.2)	2.1 / 0.05
Superior Temporal	22.6 (2.2)	24.8 (2.2)	-7.5 / <0.0001
Middle Temporal	14.2 (1.9)	15.5 (2.1)	-2.6 / 0.02
Intraparietal	26.0 (1.7)	26.0 (2.1)	n.s.
Transverse Occipital	17.2 (1.9)	16.4 (2.3)	n.s.
Calcarine Fissure	20.2 (3.2)	20.8 (3.5)	n.s.
Superior Parietal	13.3 (1.7)	14.3 (1.3)	-2.9 / 0.008
Parieto-occipital Fissure	18.8 (2.6)	20.5 (2.6)	-2.9 / 0.007
Supramarginal	21.9 (2.2)	21.1 (3.6)	n.s.
Orbitofrontal	9.6 (1.3)	10.8 (1.0)	-4.7 / <0.0001
Ant. Ascending Ramus	29.7 (2.8)	27.3 (2.2)	4.8 / <0.0001
Ant. Horizontal Ramus	13.3 (1.7)	16.2 (3.3)	18.5 / <0.0001

Table 7: One-way ANOVA test showing developmental differences between lGI for different radius (mm) within different regions.

Brain Region	LGI r=20		LGI r=25		LGI r=30		LGI r=35	
	Left $F_{2,23}$/p	Right $F_{2,22}$/p	Left $F_{2,24}$/p	Right $F_{2,24}$/p	Left $F_{2,24}$/p	Right $F_{2,24}$/p	Left $F_{2,24}$/p	Right $F_{2,24}$/p
Frontal	5.7/0.01	3.1/0.07	2.7/0.09	2.5/0.10	3.4/0.05	2.9/0.07	3.7/0.04	3.0/0.07
Parietal	9.1/0.001	5.2/0.01	7.7/0.003	3.0/0.07	6.1/0.007	4.4/0.02	6.3/0.006	4/0.03
Temporal	5.1/0.01	4.5/0.02	3.2/0.06	2.5/0.10	2.6/0.10	3.4/0.05	1.9/0.2	3.3/0.06
Medial Temporal	0.4/0.7	4.5/0.02	0.3/0.7	1.6/0.2	0.5/0.6	1.5/0.2	0.3/0.8	1.1/0.3
Occipital	2.2/0.1	1.5/0.3	2.5/0.1	1.5/0.2	2.9/0.07	1.2/0.3	2.7/0.09	2.1/0.1
Cingulate	5.8/0.009	3.7/0.04	4.7/0.02	4.6/0.02	4.3/0.03	5.6/0.01	4.6/0.02	4.3/0.03

Table 8: One-way ANOVA test showing differences of lGI between radius (mm) for each age group in each region.

Brain Region	Agegroup(8-12)		Agegroup(13-15)		Agegroup(16-19)	
	Left $F_{3,20}$/p	Right $F_{3,20}$/p	Left $F_{3,35}$/p	Right $F_{3,35}$/p	Left $F_{3,40}$/p	Right $F_{3,39}$/p
Frontal	9.1/0.0005	11.5/0.0001	7.7/0.0004	8.1/0.0003	6.5/0.001	10.9/0
Parietal	11.3/0.0001	6.4/0.003	5.8/0.002	10.0/0	6.5/0.001	11.8/0
Temporal	6.6/0.003	9.3/0.0005	6.9/0.001	9.96/0	7.4/0.0005	19.8/0
Medial Temporal	0.06/0.98	0.3/0.8	0.23/0.9	1.6/0.2	0.3/0.8	0.2/0.9
Occipital	1.8/0.2	1.0/0.4	0.13/0.9	2.1/0.1	0.49/0.7	0.5/0.7
Cingulate	1.5/0.3	0.76/0.5	0.98/0.4	1.3/0.3	2.3/0.1	2.1/0.1

Figure 1: Flow chart of the main steps of our proposed GI computation algorithm. Each figure explains the major steps of our algorithm:

(a) Pial surface extraction
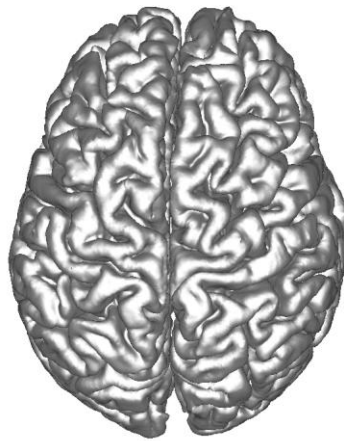
(b) Outer hull surface computation
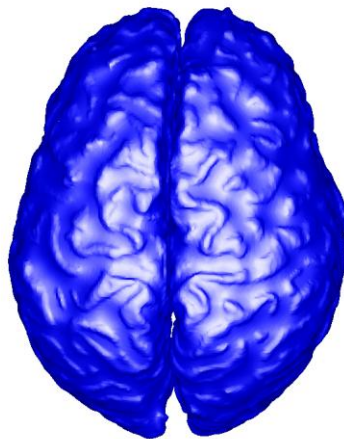
(c) Geodesic depth computation
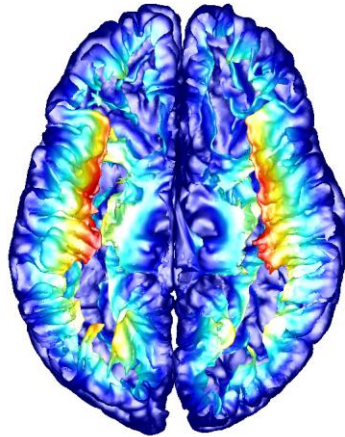
(d) Region of interest on the pial surface selection
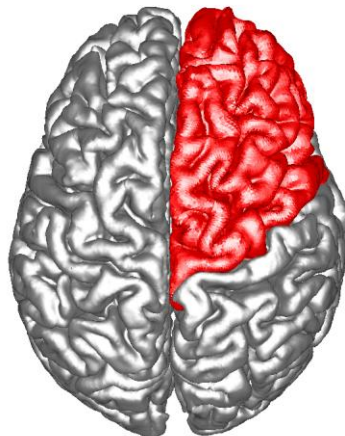
(e) Corresponding region on the outer hull surface computation
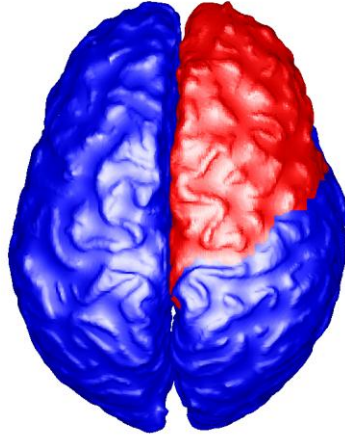
Figure 2: Axial, coronal, and sagittal slices of the MRI brain volume combined with the pial and outer hull surfaces of one hemisphere (blue lines). The red part on the curve is the intersection of the selected region (frontal lobe here) on the pial surface and the corresponding region on the outer hull surface. Top three slices correspond to Figure 1(d) (pial surface) and bottom three slices correspond to Figure 1(e) (outer hull).

Figure 3: 6 regions on left pial surface, inflated left pial surface, and the left hull surface. Frontal lobe is shown in blue, parietal lobe in green, medio temporal lobe in cyan, occipital lobe in red, and cingulated cortex in magenta. The region which is not classified is shown in brown.
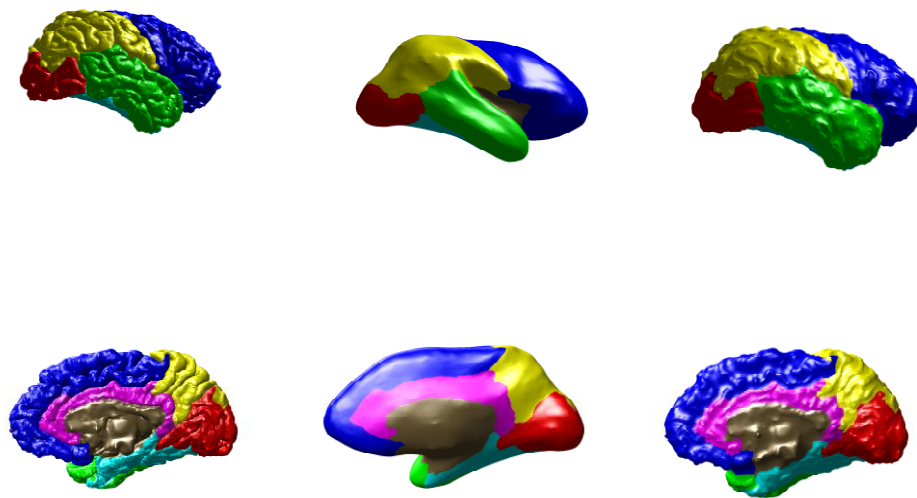
Figure 4: Area definition at a vertex. For the vertex at the center (cyan), the area is defined as the total area of the region shown in magenta, which is made up of all the triangles constructed by connecting the vertex (cyan), the centroid (black) of its neighboring triangle and the middle point (yellow) of its neighboring ring in the same triangle.
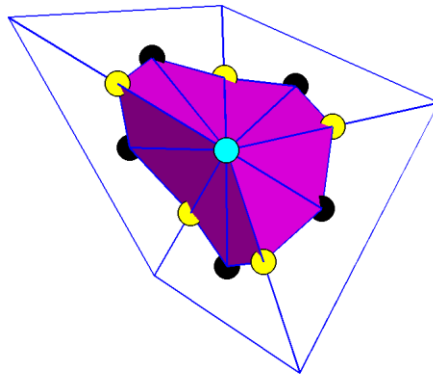
Figure 5(a): Area ratio of each region on both hemispheres for subjects in the control group. Left hemisphere measurements are marked by '+', and right hemisphere measurements are marked by '*'.
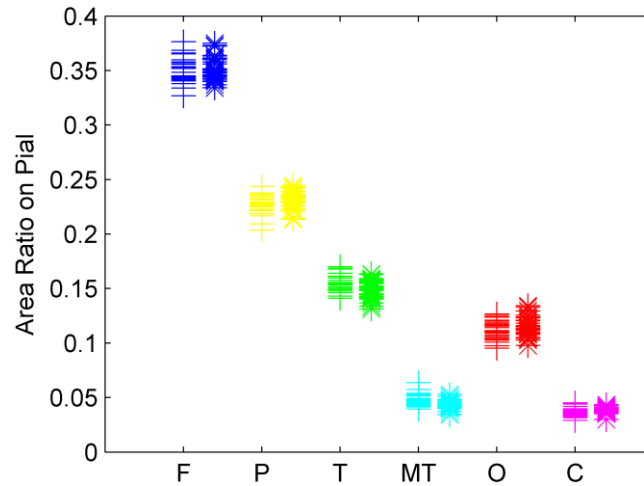

Figure 5(b): Normalized average depth of each region on both hemispheres for all subjects. Left hemisphere measurements are marked by '+', and right hemisphere measurements are marked by '*'.
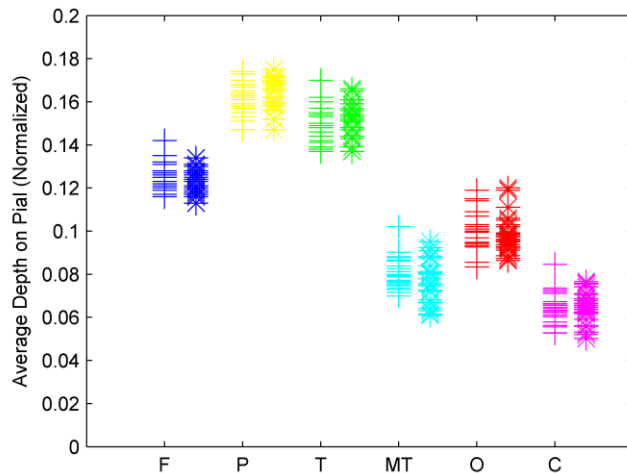
Figure 6: Area ratio of the corresponding region for each region on both hemispheres for all subjects. Left hemisphere measurements are marked by '+', and right hemisphere measurements are marked by '*'.
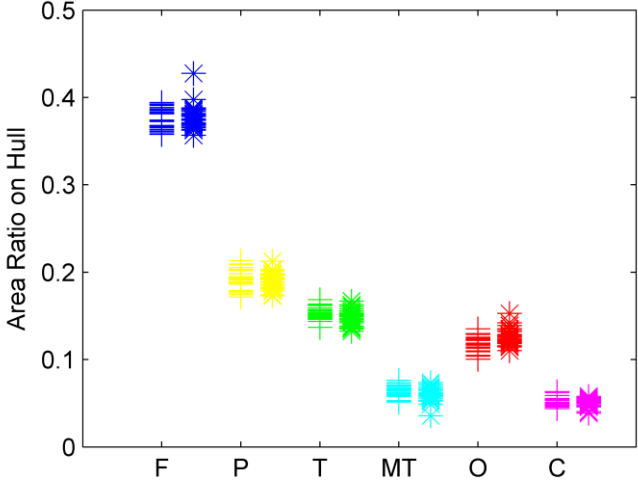
Figure 7: Developmental differences between gyrification indices within different regions for the both hemispheres.